Renewable Energy xxx (2010) 1–9

Contents lists available at ScienceDirect

Renewable Energy

journal homepage: www.elsevier.com/locate/renene

# Practical models to estimate horizontal irradiance in clear sky conditions: Preliminary results

Germán A. Salazar [a,b,*], Alejandro L. Hernández [a,b], Luis R. Saravia [a,b]

[a] Department of Physics, School of Exact Sciences, National University of Salta, Bolivia Avenue #5150, 4400 Salta Capital, Argentina
[b] INENCO (Institute of Non Conventional Energy Research), Bolivia Avenue #5150, 4400 Salta Capital, Argentina

ARTICLE INFO

*Article history:*
Received 6 November 2009
Accepted 13 January 2010
Available online xxx

*Keywords:*
High altitude sites
Horizontal irradiance model
Clear sky model
Andean region

ABSTRACT

The Argentinean Northwest (ANW) is a high altitude region located alongside Los Andes Mountains. The ANW is also one of the most insolated regions in the world due to its altitude and particular climate. However, the characterization of the solar resource in the region is incomplete as there are no stations to measure solar radiation continuously and methodically. With irradiance data recently having been measured at three sites in the Salta Province, a study was carried out that resulted in a practical model to quickly and efficiently estimate the horizontal irradiance in high altitude sites in clear sky conditions. This model uses the altitude above sea level ($A$) as a variable and generates a representative clearness index as a result ($k_{t\text{-R}}$) that is calculated for each site studied. This index $k_{t\text{-R}}$ is then used with the relative optical air mass and the extraterrestrial irradiance to estimate the instantaneous clearness index ($k_t$). Subsequently, the index $k_{t\text{-R}}$ is corrected by introducing the atmospheric pressure in the definition of relative optical air mass proposed by Kasten. The results are satisfactory as errors in the irradiance estimations with respect to measured values do not exceed 5% for pressure corrected air masses $AM_c < 2$. This model will be used in a feasibility study to locate sites for the installation of solar thermal power plants in the ANW. A prototype of a CLFR solar power plant is being built in the INENCO Campus, at the National University of Salta.



## 1. Introduction

Solar energy is a renewable energy source that is beginning to be exploited to generate massive amounts of electric energy. Solar thermal power plants have been built worldwide using the best known designs: parabolic, power tower, dish and compact linear Fresnel reflectors (CLFR) [1].

A very important aspect in the design of any thermal power plant is the evaluation of the solar resource [1–4]. For CLFR systems, this information leads to the modeling of atmospheric transmittance and the calculation of the direct normal irradiance [5]. This will determine the influence of atmospheric parameters, such as aerosols and clouds, in the rate of steam production.

The ANW is included within one of the most insolated zones on Earth and certainly in the Americas (Fig. 1). This extremely insolated region can be found in Argentina, Chile, Bolivia and Peru, amongst others. These are developing countries and lack both the necessary instruments and budget for the detailed and systematic study of the characteristics of the solar radiation incident on the region. Despite this disadvantage, many local researchers have made significant efforts to remedy this lack of information through studies in small areas coupled with extrapolation of the results to larger areas. This is the methodology used in this work.

To characterize the incident solar radiation in the area belonging to Argentina, an empirical model was developed to estimate the horizontal irradiance (and irradiation) for clear skies using as independent variables; the altitude $A$ above sea level, the geographical coordinates and the day of the year. This model emerges from the irradiance data taken for at least a year at three sites within the ANW: Salta City, Tolar Grande and El Rincon Salar, shown in Fig. 1.

While there are many ways to estimate solar radiation (by isotropic models [6–8], anisotropic models [9–16] or atmospheric radiative transfer models [17–20]), local researchers often lack the data necessary to introduce such models (air transmittance, absorption coefficients, water vapor column and diffuse radiation factors). The presented models are useful and efficient tools to obtain accurate values of horizontal global solar irradiance in a fast and easy way.

* Corresponding author.
*E-mail address:* germansalazar.ar@gmail.com (G.A. Salazar).

0960-1481/$ – see front matter © 2010 Elsevier Ltd. All rights reserved.
doi:10.1016/j.renene.2010.01.033

**Nomenclature**

| | |
|---|---|
| $\theta_z$ | Zenith solar angle |
| $A$ | Altitude above sea level (meters). |
| AM | Relative optical air mass, defined as $1/\cos\theta_z$ |
| $AM_c$ | Atmospheric pressure corrected for relative optical air mass $AM_K$ |
| $AM_K$ | Relative optical air mass, as defined by Kasten (1966) |
| $G$ | Horizontal global irradiance ($W/m^2$) |
| $G_0$ | Horizontal global extraterrestrial irradiance ($W/m^2$) |
| $G_{e,i}$ | $i$th estimated horizontal global irradiance value ($W/m^2$), obtained using the $i$th measured $G_i$ irradiance value and altitude $A$. The minimum value of RMSE between these irradiances determines the value of the constant $c_1$, which in turn determines the value of $k_{t\text{-R}}$ |
| $H$ | Daily horizontal global solar irradiation ($MJ/m^2$) |
| $H_0$ | Daily horizontal global extraterrestrial solar irradiation ($MJ/m^2$) |
| $K_t$ | Daily clearness index |
| $k_t$ | Instantaneous clearness index |
| $k_{t\text{-R}}$ | Altitude representative clearness index, obtained using AM air mass |
| $k_{t\text{-R-p}}$ | Altitude representative clearness index, obtained using $AM_c$ air mass |

Other aspects considered in this study of solar radiation, such as, daily and instantaneous clearness index definitions, atmospheric transmission coefficients and some issues of solar geometry will be discussed as they arise.

## 2. General characteristics of solar resource in the region

There are four areas in the world that exhibit the highest mean values of global horizontal solar irradiation: Africa, Australia, North and South America [21]. Except for South America, the other continents have thermal power plants in various stages of installation and tuning. INENCO has begun to build the first native CLFR system for massive electricity generation. In parallel, a quantitative study of the solar resource of the region has begun with the aim of determining the best places to install the final version of the CLFR prototype.

In Fig. 1, the region showed in the red square includes the west side of Jujuy Province, the central and west side of Salta province and the north of Catamarca Province, all in ANW. This zone, called JSC in this paper (highlighted in white in Fig. 1), is characterized by its high altitude (over 1000 m). In the Solar Energy Atlas of Argentina (SEAA) [22], the annual average monthly global irradiation in the JSC zone is approximately 5.83 $kWh/m^2$; this is equivalent to 2.13 $MWh/m^2$ per year.[1] The hours the sun is shining (sunshine hours or heliophany) is also high: the annual daily average is 8.5 h. In the SEAA, the geographic distribution of the monthly global iso-irradiation lines was calculated using the kriging method [23], but if solar irradiation or irradiance values for a specific site inside the region are needed, a new estimation method would be necessary. The empirical models presented here tries to fulfill this characterization using the altitude $A$ above sea level as the main variable.

[1] The solar energy that impinges on an area of 41 $km^2$, in the JSC zone, would be sufficient to meet the entire annual needs of Argentina.

However, not only the solar resource must be taken into account in order to decide the location of a solar thermal power plant. The proximity to power grids, roads, towns and sources of soft water, the weather, the environmental impact, etc, are all important factors to be considered [5]. There is a need for a feasibility analysis with all the information available on actual or estimated irradiance data to avoid errors in logistics and designs. The empirical model estimates global solar irradiance on sites that have been previously identified as potential or feasible for their proximity to the basic infrastructure mentioned above.

After this selection, measurements of direct and global solar radiation along with meteorological parameters must be performed in the pre-chosen places. This allows characterizing the attenuation by aerosols and determining the frequency of cloud cover and general behavior of meteorological variables.

## 3. The empirical high altitude irradiance model: definitions and premises

The possibility of estimating horizontal irradiance values using only two simple equations was recently proposed for Bogotá City [24]. The capital of Colombia is located 2580 m above sea level. Quoting other researchers [25,26], Forero et al. [24] proposed an empirical equation to estimate the instantaneous clearness index $k_t$ and/or the global irradiance $G$ on horizontal surfaces as

$$k_t = \frac{G}{G_0} = 0.7^{AM^{0.678}} \tag{1}$$

where AM is the relative optical air mass estimated as $1/\cos\theta_z$, $\theta_z$ is the zenith angle, $G$ is the measured horizontal global irradiance and $G_0$ is the horizontal extraterrestrial global irradiance. Forero et al. [24] noted that equation (1) gives very good results for measurements taken at sea level, but at higher altitudes the correlation decreases. Equation (1) is valid only for sites at sea level.

Under clear sky conditions, the attenuation of solar radiation is caused by the effects of absorption + dispersion. These effects can be considered together by using Lambert–Beer–Bouguer law [27]. To study changes in the attenuation by absorption + dispersion due to changes in altitude, Forero et al. [24] proposed a new relation, shown in equation (2), which maintains the form of equation (1) and adds terms similar to those used in Lambert–Beer–Bouguer law. In equation (2), it is assumed that the spectral coefficients of dispersion and absorption are indistinguishable for a clear atmospheric day [24].

$$k_t = \frac{G}{G_0} = \left(1 - e^{-\left(c_1 A + \tau^a + \tau^d\right)}\right)^{AM^{0.678}} = \left(1 - e^{-(c_1 A + c_2)}\right)^{AM^{0.678}} \tag{2}$$

where $c_1$ is a constant that multiplies the altitude $A$ of the site of measurement and $c_2$ is a constant related to the values of the broadband integrated spectral optical thickness coefficients $\tau^a$ for absorption and $\tau^d$ for dispersion.

The terms “absorption” and “dispersion” are related to the effects that occur in extraterrestrial solar radiation when it passes through Earth's atmosphere. The term “reflected” might be considered more accurate than “dispersion” as it refers to the solar radiation coming from the whole sky, but as this paper does not separate the measured global radiation in direct and diffuse components, we continue using the term “dispersion” to engage the atmospheric effects, over extraterrestrial solar radiation, that generate the diffuse solar radiation.

The main idea is that expression $1 - e^{-(c_1 A + c_2)}$ is a type of *corrected-by-altitude* instantaneous clearness index related to the absorption + dispersion coefficients of the Lambert–Beer–Bouguer law, broadband integrated. The goal of equations (1) and (2) is to

Please cite this article in press as: Salazar Germán A, et al., Practical models to estimate horizontal irradiance in clear sky conditions: Preliminary results, Renewable Energy (2010), doi:10.1016/j.renene.2010.01.033

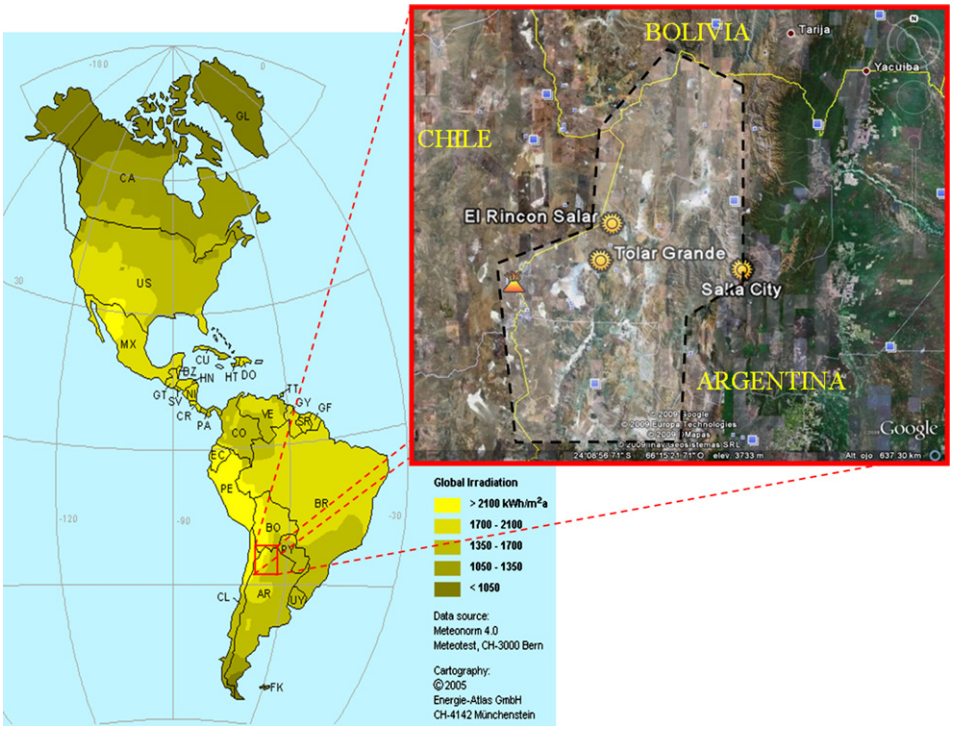


**Fig. 1.** Insolation map of America: brighter tones indicate higher insolation (Meteonorm, 2004). The studied sites are marked in the red square (sun pins).

characterize, for clear sky conditions, the processes of solar radiation attenuation by atmospheric absorption + dispersion from a wavelength-integrated point of view. In every case the measured irradiance was global horizontal irradiance sensed, using thermal or PV pyranometers.

Good quality horizontal global solar irradiance was obtained recently from reliable sources: for at least one year, irradiance values were taken in 3 sites inside the JSC region. These sites were:

(i) *Tolar Grande* (S 24.63°, W 67.33°, 4610 m). Located in Los Andes department in Salta province (Argentina), it is a scientific research station dedicated to the study of atmospheric transmittance for astronomy. Sensor used: Licor Li-200. Tolar Grande will be identified as TG in this paper.

(ii) *El Rincon Salar* (S 23.97°, W 67.11°, 3730 m). Also located in Los Andes department, it is a weather station that belongs to the Australian mining company ADY Resources Inc. Sensor used: Vaisala QMS 101. El Rincon Salar will be identified as ERS in this paper.

(iii) *Salta City* (S 24.78°, W 65.40°, 1190 m). The capital city of Salta province. Two stations provide the data: one belonging to the National Weather Service of Argentina (Servicio Meteorológico Nacional), the other belonging to INENCO. Sensor used: Kipp & Zonen CM3. Salta City will be identified as SLA in this paper.

Irradiance data were obtained from three additional sites to test the behavior of the models. These sites were as follows:

(iv) *Huacalera* (S 23.42°, W 65.35°, 2680 m). Located in the Tilcara department, in the Jujuy Province (Argentina). The data were taken by INENCO researchers. Sensor used: Kipp & Zonen CM3. Huacalera will be identified as HU in this paper.

(v) *Buenos Aires City Observatory* (S 34.58°, W 58.48°, 25 m). Is located in the capital city of the Argentina Republic. Sensor used: Kipp & Zonen CM 11. Buenos Aires City will be identified as BAC in this paper.

(vi) *El Maitén* (S 42.05° W 71.16°, 720 m). Is located in the Chubut Province, in northern Patagonia. Sensor used: PV sensor of a DAVIES automatic station. El Maitén will be identified as EM in this article.

In recent works it has been shown that the type, balance, calibration and use made of pyranometers should be carefully determined [4,28]. In this paper it is assumed that the data used was obtained from sensors previously calibrated against secondary standard instruments, so the pyranometers are assumed to involve a measurement error of 5%. The pyranometers used by INENCO (Kipp & Zonen CM3) were calibrated against a Kipp & Zonen CM21.

As mentioned before, the accuracy and balance of the sensors used in these solar radiation measurements are the best available for high altitude sites in Argentina. It must be emphasized that there are very few systematic measurements made in the region of the Andes. SWERA (Solar and Wind Energy Resource Assessment) is a programme that provides easy access to high quality renewable energy resource information and data to users all around the world, its web page contains solar radiation data from the JSC region, generated by NREL (National Renewable Energy Laboratory) physical models, but there no exits data systematically measured in the region and the NREL physical model estimations may be inaccurate. In fact the values of monthly irradiation in NREL database have 12.9% percentage RMSE compared with data measured at ERS.

The quality of measurements taken at TG, ERS and EM is directly related to the needs of the institutions that install the solar radiation sensors. According to recent studies [4] these irradiance measurements could be considerate as suboptimal, useful only for engineering purposes. Fortunately, this is the purpose of this model, and thus the accuracy of the sensors used was considered sufficient.

In equation (2) the value of AM can be determined from the value of the zenith angle $\theta_z$. This determination requires knowing

Please cite this article in press as: Salazar Germán A, et al., Practical models to estimate horizontal irradiance in clear sky conditions: Preliminary results, Renewable Energy (2010), doi:10.1016/j.renene.2010.01.033

the day $d$ of the year, the geographical coordinates of the particular site where the measurements were taken and the hour of the measurement, because the cosine of zenith angle $\theta_z$ depends on the declination, the latitude and the hour angle [29].

One important assumption made by Forero et al. [24] was that equation (2) must be equal to equation (1) at $A = 0$ m. It immediately follows that the constant $c_2$ is equal to 1.2039. The value of $e^{-1.2039}$ is 0.3 and this number, multiplied by $G_0$, can be seen as the amount of extraterrestrial solar irradiance that was lost due to the absorption + dispersion process in the path through the atmosphere. Considering the sea level altitude case and AM = 1, equation (2) remains

$$k_t = \frac{G}{G_0} = \left(1 - e^{-1.2039}\right)^{1^{0.678}} = (1 - 0.3)^{1^{0.678}} = 0.7^{1^{0.678}} = 0.7 \qquad (3)$$

The value 0.7 can be seen as the common value of clear sky instantaneous clearness index $k_t$ for all sites at the same altitude considered, measured at AM = 1. This common instantaneous clearness index allows calculating the instantaneous indexes $k_t$ values for all the moments of a day, varying only the air mass value.

Thus, the entire term $1 - e^{-(c_1 A + 1.2039)}$ indicates an *altitude representative instantaneous clearness index*, denoted as $k_{t\text{-R}}$, common to all the sites located at the same altitude $A$. By introducing the representative clearness index $k_{t\text{-R}}$ in equation (2) the following equation results

$$k_t = \frac{G}{G_0} = \left(1 - e^{-(c_1 A + 1.2039)}\right)^{\mathrm{AM}^{0.678}} = k_{\text{t-R}}^{\mathrm{AM}^{0.678}} \qquad (4)$$

Thus, a simple and practical relationship between the *altitude representative clearness index* $k_{t\text{-R}}$ and the instantaneous clearness index $k_t$ is obtained. The values of $k_{t\text{-R}}$, as function of the altitude $A$, now must be derived from the measured irradiance data.

### 3.1. Determinig the $c_1$ value for different altitudes

The next step to determine the $k_{t\text{-R}}$ values at different altitudes is to find the values of $c_1$ related to the irradiance data measured at different altitudes. If the geographic and time data are inaccurate, there will be a gap between the simultaneous values of $G_0$ and $G$, which will generate an error that will propagate to subsequent operations.

The election of the $c_1$ value for a particular site was made following mathematical methods supported by graphical information of irradiance. Only clear sky days were selected to determine the $c_1$ value. A clear sky day is a day where the graph of irradiance $G$ as a function of time $t$, when it is considered between sunrise and sunset, is a parabola. Fig. 2a and b show graphics of measured irradiance $G$ vs. time $t$ compared with parabolas that are related with the expected irradiance for a clear sky day. In fact, the evolution of the irradiance $G$ value is not a parabola equation but a cosine function. In Fig. 2a the graph of $G$ vs. $t$ is far from being a parabola, so this day was not classified as a clear sky day. The case shown in Fig. 2b is almost a perfect parabola: this was classified as a clear sky day. This is the graphical meaning of a clear sky day used in this paper. This classification method was used to support the traditional mathematical methods explained further.

Every $i$th irradiance $G_i$ value measured was related to an $i$th extraterrestrial irradiance $G_{0,i}$ value calculated as [29]

$$G_{0,i} = 1367\ \mathrm{W/m^2}\left[\left(1 + 0.033\cos\left(\frac{2\pi}{360}(d-2)\right)\right)\cos\theta_{z,i}\right] \qquad (5)$$

The value of the solar constant is 1367 W/m$^2$. The definition of the $i$th zenith angle $\theta_{z,i}$ is the same as for AM in equation (1).

Having already calculated the values of $H$ and $H_0$ for each day, some method must be used to classify the cloudiness, observing the $K_t$ values. In principle, the daily clearness index $K_t$ was used to detect the clear days: a day with a $K_t > 0.7$ can be considered as a clear sky day [30]. This old convention was used to determine, early in the analysis, which daily irradiance data will be used and which will be discarded according to what was established regarding the inclusion of only clear days in determining $c_1$. So in this first filter, the days with $K_t < 0.7$ were rejected.

Inspecting the $G$ vs. $t$ graphs of these apparently clear sky days, a problem appeared when several days firstly classified as clear sky ones revealed $G$ vs. $t$ graphics corresponding to partially cloudy days (see Fig. 3a–c). This happened in many graphs from ERS and TG. To find these non-detected partially cloudy days in the irradiance database, all the days that passed the first filter were individually inspected again, those with graphs far from being a parabola were rejected. From this analysis, it became apparent that a new sky cloudiness classification based in daily clearness index $K_t$ value would be necessary.

With the irradiance data from only clear sky days, an estimated irradiance value $G_{e,i}$ was calculated for each $i$th measured clear sky irradiance $G_i$. The expression of this $G_{e,i}$ was

$$G_{e,i} = G_{0,i}\left(1 - e^{-(c_1 A + 1.2039)}\right)^{\mathrm{AM}^{0.678}} \qquad (6)$$

where $G_{0,i}$ was calculated with equation (5).

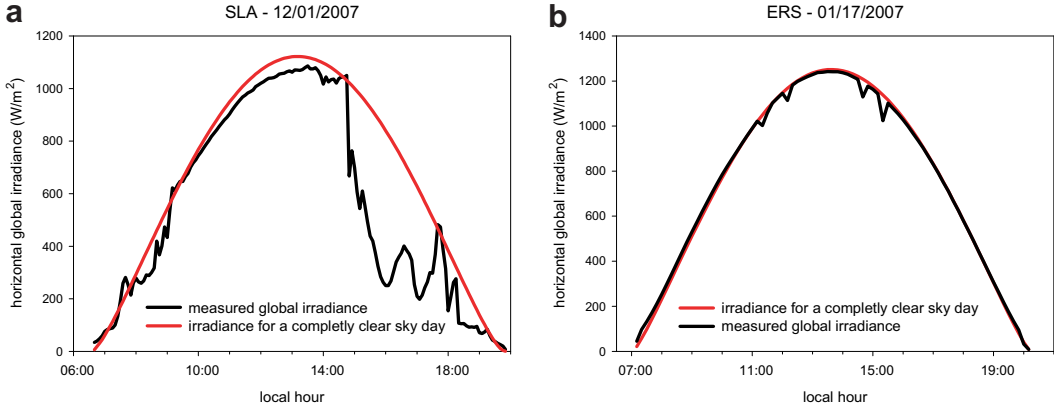


**Fig. 2.** a. Comparison of irradiance graphics between a theoretical clear day (red line) and a measured non-clear day (black line). b. Comparison between two clear days: one measured (black line) and one estimated (red line). (For interpretation of the references to colour in this figure legend, the reader is referred to the web version of this article).

Please cite this article in press as: Salazar Germán A, et al., Practical models to estimate horizontal irradiance in clear sky conditions: Preliminary results, Renewable Energy (2010), doi:10.1016/j.renene.2010.01.033

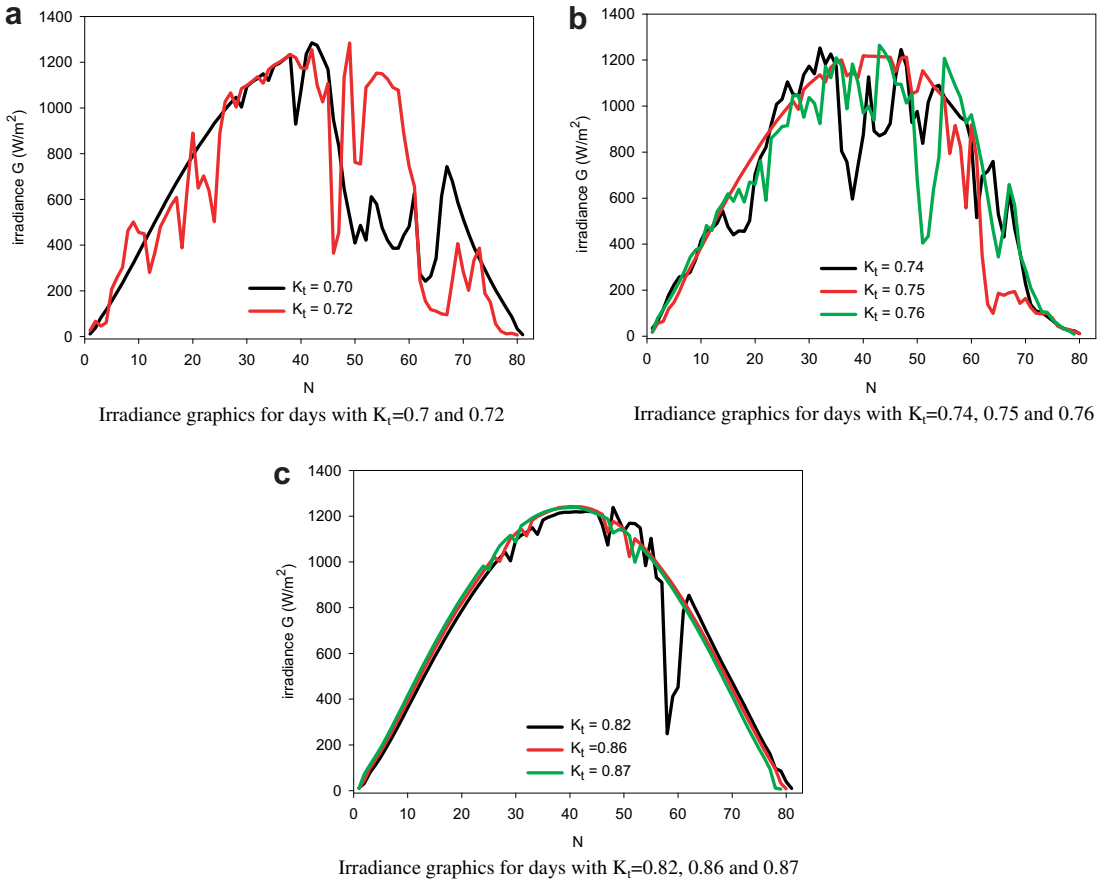


**Fig. 3.** (a–c). Horizontal global irradiances measured in ERS. The $K_t$ values are higher than 0.7 but the graphs $G$ vs. $t$ indicate a partially cloudy day.

For all the $G_i$ and the estimated $G_{e,i}$ values measured at a site, a Root Mean Square Error (RMSE) was calculated. The value of the RMSE was the statistic tool employed to search for the $c_1$ value; the value that minimized the RMSE was chosen as the searched value.

$$\text{Minimum } \frac{\sqrt{\sum_{i=1}^{M}\left(G_i - G_{e,i}\right)^2}}{M} \Rightarrow c_1 \tag{7}$$

where $M$ is the total amount of clear sky irradiance measurements at a particular site. The time steps used in the measurements done for TG, ERS and EM was 10 min, in SLA it was 15 min until June of 2007 when it was increased to 5 min, in HU it was 15 min and in BAC, 60 min. The $M$ values corresponding to each site are shown in Table 1.

This value of $c_1$ allows calculating the *altitude representative clearness index* for the site whose irradiance data was processed, characterized by the altitude. Table 2 lists the results obtained performing this procedure with the filtered irradiance data. The Media Bias Error (MBE) was also calculated. The $k_{t\text{-R}}$ were taken to 4 decimals instead of the traditional 2 because $c_1$ is very small and significant variations in it produce changes in the $k_{t\text{-R}}$ values that cannot be assessed correctly with only 2 decimals.

These $k_{t\text{-R}}$ values allow determining the instantaneous $k_t$ values for any day in each particular site. For each site studied the equation (4) now could be written as follows:

$$\text{TG}(4609\ \text{m})\ k_t = 0.9113^{\text{AM}^{0.678}} \tag{8}$$

$$\text{SER}(3730\ \text{m})\ k_t = 0.8885^{\text{AM}^{0.678}} \tag{9}$$

$$\text{SLA}(1190\ \text{m})\ k_t = 0.7986^{\text{AM}^{0.678}} \tag{10}$$

It can be seen that as the altitude increases, the altitude representative clearness index $k_{t\text{-R}}$ gets larger. This is consistent with the fact that at greater altitudes there is a minor effect of atmospheric absorption + dispersion attenuation in the solar radiation, than for lower altitudes. The reason being that at high altitudes the solar

**Table 1**
Number of clear irradiance measurements contained in the remaining filtered days.

| Site | Number of clear sky irradiance measurements ($M$) |
|---|---|
| TG | 14,312 |
| ERS | 13,619 |
| HU | 3,456 |
| SLA | 7,559 |
| EM | 1,258 |
| BAC | 1,128 |

**Table 2**
Values of $c_1$ and $k_{t\text{-R}}$ for the high altitude sites studied. The RMSE and the MBE were also calculated.

| Site | Altitude (m) | $c_1$ ($m^{-1}$) | Measured $k_{t\text{-R}}$ | RMSE ($W/m^2$) | MBE ($W/m^2$) |
|---|---|---|---|---|---|
| TG | 4609 | $2.644 \times 0^{-4}$ | 0.9113 | 24 | 2 |
| ERS | 3730 | $2.653 \times 10^{-4}$ | 0.8885 | 29 | 2 |
| SLA | 1190 | $3.350 \times 10^{-4}$ | 0.7986 | 33 | 3 |

Please cite this article in press as: Salazar Germán A, et al., Practical models to estimate horizontal irradiance in clear sky conditions: Preliminary results, Renewable Energy (2010), doi:10.1016/j.renene.2010.01.033

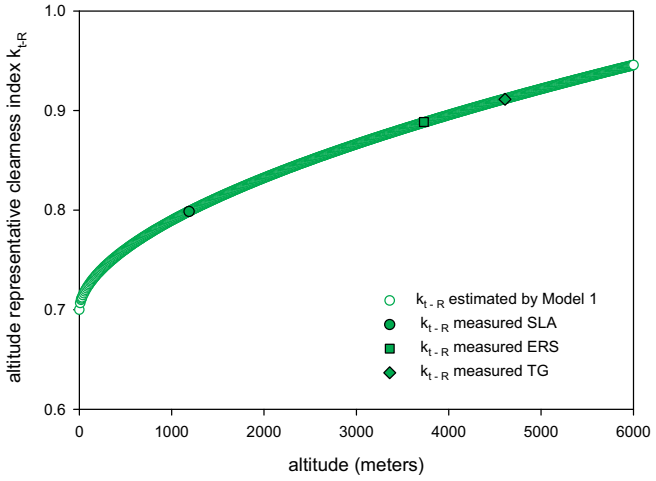


**Fig. 4.** Model 1 predicted and measured $k_{t\text{-}R}$ for TG, ERS and SLA. When $A = 0$ m, $k_{t\text{-}R} = 0.7$.

radiation has less atmosphere to interact with. Thus, the physical effect of the solar radiation attenuation due to atmospheric absorption + dispersion is described mathematically. This is the only physical approach used in this work, based on averaged observations of clear sky days.

At this point, there are only three measured $k_{t\text{-}R}$ values related to only three different altitudes. To find a relationship that could predict $k_{t\text{-}R}$ values for intermediate altitudes and determine whether this is consistent with other measured irradiance data, a regression calculation was performed. The equation of the curve that more accurately fits the points in Cartesian coordinates ($x = A$, $y = k_{t\text{-}R}$) from Table 2 was a power function shown in equation (11):

$$k_{t\text{-}R} = 0.7 + 1.8328 \times 10^{-3} . A^{0.5630} \quad (11)$$

The correlation coefficient is $R^2 = 0.9999$. For altitude $A = 0$ m it was considered that $k_{t\text{-}R} = 0.7$, following the starting premise pointed by Forero et al. [24]. Fig. 4 shows the estimated $k_{t\text{-}R}$ for altitudes between 0 and 6000 m, as well as the measured $k_{t\text{-}R}$ in each site.

Evidently, the most important expression of equation (4) is the $k_{t\text{-}R}$ definition and in equation (11), $k_{t\text{-}R}$ is shown as function of the altitude $A$; therefore, the $k_{t\text{-}R}$ expression will be directly called a "model". We will refer to equation (11) as *Model 1.*

Despite the very good result of the correlation coefficient, it was necessary to determine the errors in estimation of Model 1 because $k_{t\text{-}R}$ will be used to calculate every $k_t$ for a day. The measured $k_{t\text{-}R}$ and the estimated values by Model 1 are compared in Table 3. In every case the percentage difference P.D. is less than 0.07%.

It is important to test the behavior of Model 1 using irradiance values measured at different altitudes. To do this, irradiance data from HU and BAC were obtained. Table 4 lists the measured $k_{t\text{-}R}$ in these two sites compared to Model 1 predictions. The irradiance data from BAC was collected during 2003. BAC is not a high altitude site, but useful to test the behavior of the Model 1 at altitudes below 1000 m. As seen in Table 4, the $k_{t\text{-}R}$ measured in BAC was higher than the Model 1 estimation. This difference could be explained if

**Table 3**
Percentage difference PD between measured and estimated $k_{t\text{-}R}$ using Model 1.

| Site | Altitude (m) | $k_{t\text{-}R}$ measured | $k_{t\text{-}R}$ Model 1 | PD (%) |
|---|---|---|---|---|
| TG | 4609 | 0.9113 | 0.9117 | −0.04 |
| ERS | 3730 | 0.8885 | 0.8879 | 0.06 |
| SLA | 1190 | 0.7986 | 0.7988 | −0.02 |
| Sea level | 0 | 0.7 | 0.7000 | 0.00 |

**Table 4**
Percentage difference between the measured $k_{t\text{-}R}$ in Huacalera and Buenos Aires City compared to Model 1 predictions.

| Site | Altitude (m) | $k_{t\text{-}R}$ measured | $k_{t\text{-}R}$ Model 1 | PD (%) |
|---|---|---|---|---|
| HU | 2680 | 0.8642 | 0.8560 | 0.95 |
| BAC | 25 | 0.7694 | 0.7112 | 7.56 |

BAC had an extremely clear atmosphere or if the starting premise for sea level altitude was incorrect ($k_{t\text{-}R} = 0.7$ at $A = 0$ m). BAC is an environmentally non-friendly megalopolis with more than 12 million inhabitants, so its atmosphere transparency conditions are of an industrial type. Therefore, the second explanation is more feasible than the first.

A new model arose when a regression was performed using the $k_{t\text{-}R}$ values from Table 2, using the $k_{t\text{-}R}$ measured for BAC for $A = 25$ m instead of the $k_{t\text{-}R} = 0.7$ for $A = 0$ m. Its expression is shown in equation (12). This is *Model 2*

$$k_{t\text{-}R} = 0.7679 + 1.4184 \times 10^{-5} . A^{1.0956} \quad (12)$$

The correlation coefficient of this expression is $R^2 = 0.9974$. Fig. 5 shows the measured $k_{t\text{-}R}$ in each site, the $k_{t\text{-}R}$ predicted by Model 1 and by Model 2.

Fig. 5 depicts the largest differences between the model's estimates for altitudes below 1000 m and above 5000 m, so it is necessary to test the models with irradiance data from a site inside the mentioned range of altitudes: 1000 m > $A$ > 5000 m. Clear sky irradiance data from a town called El Maitén (S 42.05° W 71.16°, 720 m), which is located in parallel − 42° in the north of Argentine Patagonian region, was used for this purpose. From measurements collated between January and May of 2008, the $k_{t\text{-}R}$ for this site was calculated as 0.7846. Table 5 demonstrates the values of each representative clearness index and the percentage difference between their measured and estimated values.

Model 1 offers improved results for altitudes over 1000 m and the Model 2 for altitudes under that mark. Nevertheless, it is necessary to test the models against more accurate quality irradiance data from different sites at different altitudes to determine which model is most representative or, to improve the $k_{t\text{-}R}$ expressions.

### 3.2. Variation in the models changing the air mass expression

One of the main aspects considered in the development of Model 1 and Model 2, was the definition of relative optical air mass

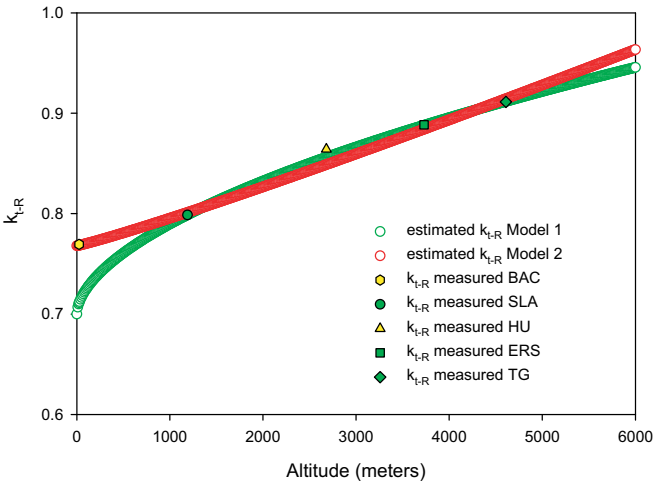


**Fig. 5.** Model 1 and Model 2 predicted and measured $k_{t\text{-}R}$ for each site.

**Table 5**
Percentage difference between the estimations of the two Models. The minor PD values between models are highlighted in italics.

| Site | Altitude (m) | $k_{t\text{-R}}$ measured | PD respect to Model 1 (%) | PD respect to Model 2 (%) |
|---|---|---|---|---|
| TG | 4609 | 0.9113 | *−0.04* | −0.33 |
| ERS | 3730 | 0.8885 | *0.06* | 0.50 |
| HU | 2680 | 0.8642 | *0.95* | 1.79 |
| SLA | 1190 | 0.7986 | *−0.02* | −0.32 |
| EM | 720 | 0.7846 | 1.30 | *−0.31* |
| BAC | 25 | 0.7694 | 7.56 | *0.13* |

AM. When the atmospheric pressure is introduced in the air mass definition, the expressions of the models change. In the widely used spectral atmosphere radiative transfer model SPECTRAL2 [17] the air mass expression, equation (14), proposed by Kasten [31] is used in conjunction with the atmospheric pressure corrected air mass $AM_c$ (equation (13))

$$AM_c = AM_K \cdot \left(\frac{P}{101355}\right) \tag{13}$$

$$AM_K = 1 \Big/ \left(\cos\theta_z + 0.15(93.885 - \theta_z)^{-1.253}\right) \tag{14}$$

This expression was used to correct the Kasten air mass $AM_K$ by atmospheric pressure. Since there are no measured atmospheric pressure data available from most of the sites, the pressure $P$ as a function of the altitude $A$, was estimated using the following expression [32]

$$P = 101355\left(\frac{288.15}{288.15 - 0.0065A}\right)^{-5.255877} \tag{15}$$

where pressure $P$ is in Pascal and altitude $A$ is in meters. In equation (15) the temperature and pressure functions used in the 1976 U.S. Standard Atmosphere are combined, which is an idealized, steady-state representation of the Earth's atmosphere from the surface to 1000 km, as it is assumed to exist in a period of moderate solar activity. The air is assumed to be dry, and at heights below 86 km, the atmosphere is assumed to be homogeneously mixed [32]. Equation (15) has provided a very close estimate (878 hPa) of the average measured value in SLA over a period of almost 2 years (879 hPa). Therefore, it can be assumed that the expression is valid for the remaining sites.

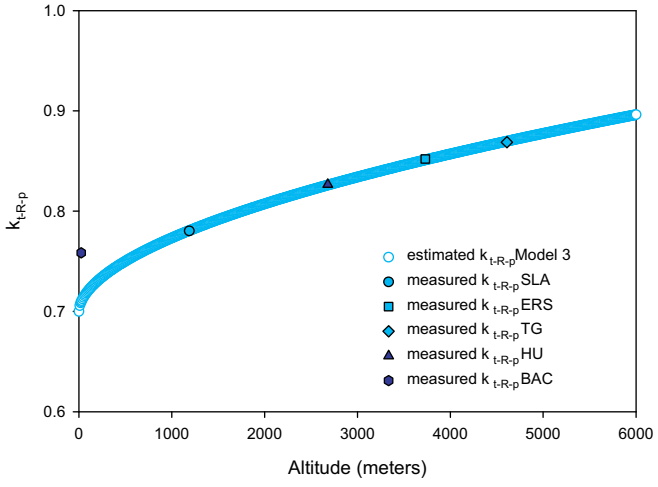


**Fig. 6.** Model 3 predicted and measured $k_{t\text{-R-p}}$. Note the value of BAC.

**Table 6**
Values of the pressure corrected $c_{1\text{-p}}$ and $k_{t\text{-R-p}}$, measured for the high altitude sites studied. The RMSE and the MBE were also calculated.

| Site | Altitude (m) | $c_{1\text{-p}}$ ($m^{-1}$) | $k_{t\text{-R-p}}$ | Estimated pressure (hPa) | RMSE ($W/m^2$) | MBE ($W/m^2$) |
|---|---|---|---|---|---|---|
| TG | 4609 | $1.795 \times 10^{-4}$ | 0.8688 | 569 | 27 | 1 |
| ERS | 3730 | $1.896 \times 10^{-4}$ | 0.8521 | 639 | 29 | 1 |
| SLA | 1190 | $2.613 \times 10^{-4}$ | 0.7802 | 879 | 26 | 2 |

Using again the method described to find Model 1, the new expression of the $k_{t\text{-R}}$, now called $k_{t\text{-R-p}}$, becomes:

$$k_{t\text{-R-p}} = 0.7 + 1.6391 \times 10^{-3} \cdot A^{0.5500} \tag{16}$$

The correlation factor is high again: $R^2 = 0.9999$. This is the expression of *Model 3*.

Fig. 6 reveals the $k_{t\text{-R-p}}$ values estimated and measured in Table 6, plus the $k_{t\text{-R-p}}$ values measured for HU and BAC. The estimations for BAC are again uncorrelated with the $k_{t\text{-R-p}}$ measured for the site (0.7584). Nevertheless, for sites between 1190 and 4610 m, the estimated values of $G$ by Models 1 and 3 are essentially the same, like the estimated $H$ and $K_t$ values. Over 4610 m, the estimations of Model 3 begin to differentiate from those of Model 1, the latter being larger than the estimates of Model 3. Hence, Model 3 should not be used to estimate irradiance values for altitudes below 1000 m: it is a high altitude irradiance/irradiation practical model. Another advantage of Model 3 over Model 1, is that it allows estimations for higher altitudes than Model 1, before reaching the maximum possible $k_{t\text{-R-p}}$ value (=1). For model 3, $k_{t\text{-r-p}} = 1$ occurs at 12990 m and for Model 1 $k_{t\text{-R}} = 1$ at 8370 m.

Table 7 shows the differences between Model 3 estimated and measured representative clearness indexes. The percentage differences P.D. are slightly larger than in Table 3. The cause of this minor difference lies in the definition of the air mass used in each model. Nevertheless, the mathematical relation between the altitude representative clearness index and the air mass is the same in Model 1 and in Model 3.

Finally, adding the pressure corrected value $k_{t\text{-R-p}}$ of BAC to the list presented in Table 7, a final model (similar to Model 2) arises: *Model 4*

$$k_{t\text{-R-p}} = 0.7570 + 1.0112 \times 10^{-5} \cdot A^{1.1067} \tag{17}$$

The correlation index is $R^2 = 0.996$.

Table 8 shows the percentage difference between Model 4 estimated and measured $k_{t\text{-R-p}}$ values. For high altitudes sites, Model 3 has less error than Model 4, however, the latter performs much better for low altitudes.

## 4. First results

Fig. 7a–d show the graphic estimations of Model 3 for different sites at different altitudes in different days. An excellent correlation can be appreciated from the figures.

**Table 7**
Percentage difference between the Model 3 estimated $k_{t\text{-R-p}}$ and the measured values.

| Site | Altitude | Measured $k_{t\text{-R-p}}$ | Estimated $k_{t\text{-R-p}}$ Model 3 | PD (%) |
|---|---|---|---|---|
| TG | 4609 | 0.8688 | 0.8697 | −0.10 |
| ESR | 3730 | 0.8521 | 0.8510 | 0.13 |
| SLA | 1190 | 0.7802 | 0.7806 | −0.05 |
| Sea level | 0 | 0.7 | 0.7000 | 0.00 |

Please cite this article in press as: Salazar Germán A, et al., Practical models to estimate horizontal irradiance in clear sky conditions: Preliminary results, Renewable Energy (2010), doi:10.1016/j.renene.2010.01.033

**Table 8**
Percentage difference PD between the Model 4 estimated $k_{t\text{-R-p}}$ and the measured values. Note the higher values of PD than in Table 7, but never greater than 1%.

| Site | Altitude | Measured $k_{t\text{-R-p}}$ | Estimated $k_{t\text{-R-p}}$ Model 4 | PD (%) |
|---|---|---|---|---|
| TG | 4609 | 0.8688 | 0.8716 | −0.32 |
| ERS | 3730 | 0.8521 | 0.8477 | 0.52 |
| SLA | 1190 | 0.7802 | 0.7826 | −0.31 |
| BAC | 25 | 0.7584 | 0.7574 | 0.13 |

## 5. Discussion

(i) For practical purposes, both Models 3 & 4 are valid for estimating irradiance at high altitude sites, but Model 4 estimate $k_{t\text{-R-p}}$ in a broad range of altitudes (0–4610 m a.s.l.) with an error less than 1%. Model 3 is remarkable because it estimates $k_{t\text{-R-p}}$ with less error than Model 4 but only for sites located at altitudes over 1000 m. Since the study of this paper is focused on estimating the irradiance and irradiation of horizontal global solar radiation in a clear sky day in the JSC zone, the advantage of Model 3 over Model 4 is obvious to the particular case analyzed.

(ii) Convention to determine the lower $K_t$ value to classify a day as a clear sky day:

It was mentioned that the determination of $c_{1\text{-p}}$ and $k_{t\text{-R-p}}$ depends strongly on whether the irradiance data used belongs to clear sky days because other types of irradiance data will generate incorrect values of $c_{1\text{-p}}$ and $k_{t\text{-R-p}}$.

In this paper the definition of clear sky day is graphic: it is a day which $G$ vs. $t$ irradiance graph is almost a perfect parabola. Analyzing the irradiance data of TG, ERS and SLA, days have been detected with values of $K_t$ above 0.7 but whose graph $G$ vs. $t$ indicates partially cloudy days. This situation occurred mainly in ERS and TG. Examples of these cases are shown in Fig. 3a and b. A new convention is needed to determine the minimum value of $K_t$ to classify a day as a clear sky one.

Model 3 was used to estimate the clear day $K_t$ values for the 15th day of every month at the three sites. This model was chosen for this purpose because it has the lower error between measured and estimated $k_{t\text{-R-p}}$ for altitudes over 1000 m. Table 9 lists the values of the $K_t$ for the 15th day of each month, for the three studied sites. In an attempt to derive a helpful mathematical expression to estimate this $K_t$ value for altitudes between 1000 and 6000 m, the last column of Table 9 shows power functions of the altitude $A$ related to the day of the year: these being calculated by mathematical regression of the $K_t$ values.

The previous convention [30] used to classify the sky cloudiness of a day based on the $K_t$ value results inaccurate when irradiance data from high altitudes sites are involved. Thus, in a site at 1190 m, the lower $K_t$ value of a day to be considered as a clear sky is 0.75 instead of 0.70 as proposed by Iqbal [30]. In a site at 4000 m, on the same date, the lower $K_t$ value of a day to be considered as a clear sky day is 0.89. As the altitude gets higher, the Iqbal convention

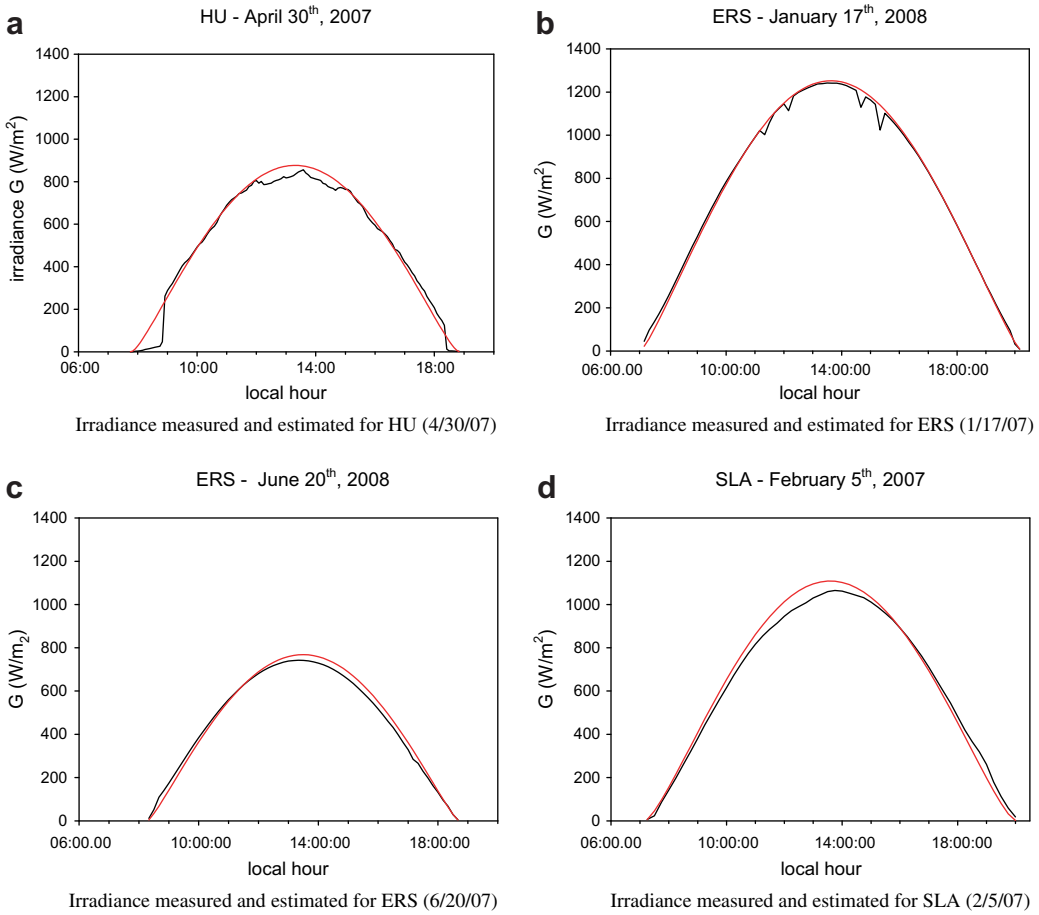


**Fig. 7.** (a–d) A comparison between measured and estimated irradiance values for different sites. The red lines show Model 3 estimations and the black depict measured irradiance values.

Please cite this article in press as: Salazar Germán A, et al., Practical models to estimate horizontal irradiance in clear sky conditions: Preliminary results, Renewable Energy (2010), doi:10.1016/j.renene.2010.01.033

**Table 9**
Calculation of the daily clearness index $K_t$ for the 15th day of each month, using Model 3. In the last column are presented expressions derived to determine the minimum $K_t$ as function of the altitude $A$.

| Day | Estimated $K_t$ | | | $K_t\,(A)$ |
|---|---|---|---|---|
| | SLA | ERS | TG | |
| 15 | 0.75 | 0.86 | 0.89 | $K_{t\,d=15} = 0.6381 + 0.001606.A^{0.5993}$ |
| 46 | 0.75 | 0.86 | 0.88 | $K_{t\,d=46} = 0.5487 + 0.01458.A^{0.3709}$ |
| 74 | 0.74 | 0.85 | 0.88 | $K_{t\,d=74} = 0.6281 + 0.001606.A^{0.5993}$ |
| 105 | 0.73 | 0.84 | 0.87 | $K_{t\,d=105} = 0.6181 + 0.001606.A^{0.5993}$ |
| 135 | 0.71 | 0.83 | 0.86 | $K_{t\,d=135} = 0.5361 + 0.006723.A^{0.4593}$ |
| 166 | 0.69 | 0.82 | 0.86 | $K_{t\,d=166} = 0.6028 + 0.000304.A^{0.7989}$ |
| 196 | 0.70 | 0.83 | 0.86 | $K_{t\,d=196} = 0.4196 + 0.02645.A^{0.334}$ |
| 227 | 0.72 | 0.84 | 0.87 | $K_{t\,d=227} = 0.5461 + 0.006723.A^{0.4593}$ |
| 258 | 0.74 | 0.85 | 0.88 | $K_{t\,d=258} = 0.6281 + 0.001606.A^{0.5993}$ |
| 288 | 0.75 | 0.86 | 0.88 | $K_{t\,d=288} = 0.5487 + 0.01458.A^{0.3709}$ |
| 319 | 0.75 | 0.86 | 0.89 | $K_{t\,d=319} = 0.6381 + 0.001606.A^{0.5993}$ |
| 349 | 0.75 | 0.86 | 0.89 | $K_{t\,d=349} = 0.6381 + 0.001606.A^{0.5993}$ |
| Max | 0.75 | 0.86 | 0.89 | |
| Min | 0.69 | 0.82 | 0.86 | |
| Average | 0.73 | 0.85 | 0.88 | |

classifies days as clear sky when in fact they belong to the partially cloudy category.

## 6. Conclusions

Models 3 & 4 are simple practical models to estimate the horizontal global solar irradiance for clear sky conditions in the ANW Andean zone. These models are based in the empirical determination of a factor called altitude representative clearness index $k_{t\text{-R-p}}$ that varies with altitude. The altitude representative clearness index $k_{t\text{-R-p}}$, raised to the quantity $AM_c^{0.678}$, is multiplied by the horizontal extraterrestrial global irradiance $G_0$ to estimate the value of the horizontal global solar irradiance $G$. All the geographical and temporal information is implicit in the extraterrestrial irradiance $G_0$ and in the air mass $AM_c$.

Model 3 offers the best irradiance estimations for altitudes above 1000 m and Model 4 for estimations between 0 and 4610 m. In general, the error of the irradiance estimations is about 5% of the measured values for relative optical air masses $AM_c < 2$.

A new method, based in Model 3 estimations, is proposed to find the clear sky days based on their daily clearness index $K_t$ value. The convention used previously was inaccurate, classifying partially cloudy days as clear ones. This new method has proved valuable in finding the clear days, but should be tested with more data to demonstrate a more general validity.

Models 3 & 4 should be improved in the future through the inclusion of more irradiance measurements and weather data from both high and low altitude sites. Model 3 aims to be a useful model for engineering purposes, and is already being used in the analysis of possible sites to install a CLFR power plant, in the Calchaquies Valleys (south-west of the province of Salta).

## Acknowledgements

A special thanks to Dr. Hugo Grossi Gallegos for providing the data of BAC, the Argentina National Weather Service (Servicio Meteorologico Nacional) for the data of SLA, the company ADY Resources Inc. for the data of ERS, Ruben Vrech for the data of TG, Dr. Miguel Condorí, Ricardo Echazú, Gonzalo Duran, Aldo Palacios, Hugo Suligoy and Carlos Fernandez for support for travels and logistics.

## References

[1] Mills D. Advances in solar thermal electricity technology. Solar Energy 2004;76:19–31.
[2] Rolim M, Fraidenraich N, Tiba C. Analytic modeling of a solar power plant with parabolic linear collectors. Solar Energy 2009;83:126–33.
[3] Yao Z, Wang Z, Lu Z, Wei X. Modeling and simulation of the pioneer 1 MW solar thermal central receiver system in China. Renewable Energy 2009;34 (11):2437–46.
[4] Gueymard C. Direct and indirect uncertainties in the prediction of tilted irradiance for solar engineering applications. Solar Energy 2009;83:432–44.
[5] Trieb F. Assessment of solar energy resources and sites by satellite remote sensing technology. In: Solar Energy Symposium (Nicosia-Cyprus), 2001. PPT available in LDR web page (Available at: <www.dlr.de>).
[6] Hottel HC, Woertz BB. Evaluation of flat-plate solar heat collector. Transactions of the ASME 1942;64:91. Cited by Duffie and Beckman, 2006.
[7] Liu BYH, Jordan RC. The interrelationship and characteristic distribution of direct, diffuse, and total solar radiation. Solar Energy 1960;4(3):1–19.
[8] Badescu V. 3D isotropic approximation for solar diffuse irradiance on tilted surfaces. Renewable Energy 2002;26:221–33.
[9] Perez R, Ineichen P, Seals R, Michalsky J, Stewart R. Modeling daylight availability and irradiance components from direct and global irradiance. Solar Energy 1990;44(5):271–89.
[10] Perez R, Stewart R, Arbogast C, Seals R, Scott J. An anisotropic hourly diffuse radiation model for sloping surfaces: description, performance validation, site dependency evaluation. Solar Energy 1986;36(6):481–97.
[11] Gueymard C. An anisotropic solar irradiance model for tilted surfaces and its comparison with selected engineering algorithms. Solar Energy 1987;38(5): 367–86.
[12] Robledo L, Soler A. A simple clear skies model for the luminous efficacy of diffuse solar radiation on inclined surfaces. Renewable Energy 2002;26: 169–76.
[13] Li DHW, Lam JC, Lau CCS. A new approach for predicting vertical global solar irradiance. Renewable Energy 2002;25:591–606.
[14] Olmo FJ, Vida J, Castro-Diez Y, Alados-Arboledas L. Prediction of global irradiance on inclined surfaces from horizontal global irradiance. Energy 1999;24: 689–704.
[15] Klucher TM. Evaluation of models to predict insolation on tilted surfaces. Solar Energy 1979;23(2):111–4.
[16] Muneer T. Solar radiation and daylight models for the energy efficient design of buildings. Oxford: Architectural Press; 1997.
[17] Bird R, Riordan C. Simple solar spectral model for direct and diffuse irradiance on horizontal and tilted planes at the earth's surface for cloudless atmospheres. Journal of Climate and Applied Meteorology 1986;25:87–97.
[18] Bird R, Hulstrom R. A simplified clear sky model for direct and diffuse insolation on horizontal surfaces. SERI; 1981. Technical Report SERI/TR-642-761.
[19] Gueymard C. SMARTS2, a simple model of the atmospheric radiativa transfer of sunshine: algorithms and perfomance assessment. Florida Solar Energy Center/University of Central Florida; 1995. FSEC-PF-270-95.
[20] Souster CG, Rodgers GG, Page JK. The development of an interactive computer program SUN3 for the calculation of solar irradiances and daily irradiations incident upon surfaces of any slope and orientation and cloudless days for given conditions of sky clarity and atmospheric water content. England: Department of Building Science. Faculty of Architectural Studies. University of Sheffield; 1978.
[21] Meteonorm. Available at: <www.meteotest.ch>; 2006.
[22] Grossi Gallegos H, Righini R. Atlas de Energía Solar de la República Argentina. In: Eds. SECYT and Universidad Nacional de Lujan (Argentina). 2007.
[23] Grossi Gallegos H, Righini R, Raichijk C. Approach to drawing new global solar irradiation contour maps for Argentina. Renewable Energy 2005;30:1241–55.
[24] Forero N, Caicedo L, Gordillo G. Correlation of global solar radiation values estimated and measured on an inclined surface for clear days in Bogotá. Renewable Energy 2007;32:2590–602.
[25] Meinel A, Meinel M. Applied solar energy, an introduction. Reading, MA: Addison-Wesley; 1976.
[26] Laue EG. The measurement of solar spectral irradiance at different terrestrial elevations. Solar Energy 1970;13(1):43–57.
[27] Platt U. Air monitoring by differential optical absorption spectroscopy. Contribution to the encyclopedia of analytical chemistry (EAC), Instrumentation and applications. John Wiley and Sons; 2001.
[28] Gueymard C, Myers D. Evaluation of conventional and high-performance routine solar radiation measurements for improved solar resource, climatological trends, and radiative modeling. Solar Energy 2009;83:171–85.
[29] Duffie J, Beckman W. Solar engineering of the thermal processes. John Wiley & Sons; 2006.
[30] Iqbal AMM. An introduction to solar radiation. Academic Press; 1983.
[31] Kasten F. A new table and approximate formula for relative optical air mass. Archives for Meteorology Geophysics and Bioclimatology 1966;B14:206–23.
[32] Lide DR. Handbook of chemistry and physics. 71st. ed. Boston: CRC Press; 1990. pp. 14.12.

Please cite this article in press as: Salazar Germán A, et al., Practical models to estimate horizontal irradiance in clear sky conditions: Preliminary results, Renewable Energy (2010), doi:10.1016/j.renene.2010.01.033